# D4.2 Assessment of hygrothermal and textural features controlling building materials decay, and required as input in the hydrothermal simulations

| | |
|---|---|
| Deliverable number | **D4.2** |
| Deliverable title | **Assessment of hygrothermal and textural features controlling building materials decay, and required as input in the hydrothermal simulations** |
| Nature[1] | **R** |
| Dissemination Level [2] | **PU** |
| Author (email)<br>Institution | **Chiara Coletti (chiara.coletti@unipd.it)**<br>**Luigi Germinario (luigi.germinario@unipd.it)**<br>**UNIPD** |
| Editor (email)<br>Institution | **Claudio Mazzoli (claudio.mazzoli@unipd.it)**<br>**UNIPD** |
| Leading partner | **UNIPD** |
| Participating partners | **IUAV, UGR** |
| Official submission date: | **31/05/2021** |
| Actual submission date: | **30/06/2021** |

[1] **R**=Document, report; **DEM**=Demonstrator, pilot, prototype; **DEC**=website, patent fillings, videos, etc.; **OTHER**=other

[2] **PU**=Public, **CO**=Confidential, only for members of the consortium (including the Commission Services), **CI**=Classified, as referred to in Commission Decision 2001/844/EC

| Modifications Index | |
|---|---|
| Date | Version |
| 07/06/2021 | 0.1 First draft by UNIPD |
| 20/06/2021 | 0.2 Second draft by UNIPD and UGR |
| 25/06/2021 | 0.3 Third draft by UNIPD, UGR, and IUAV |
| 30/06/2021 | 0.4 Last version edited by the WP leader |

This work is a part of the HYPERION project. HYPERION has received funding from the European Union's Horizon 2020 research and innovation programme under grant agreement no 821054.

# ACRONYMS AND ABBREVIATIONS

| | |
|---|---|
| CIE | Commission Internationale de l'Éclairage |
| EDS | Energy-dispersive X-ray spectroscopy |
| HRAP | Holistic Risk Assessment Platform |
| HT | Hygro-Thermal |
| MIP | Mercury Intrusion Porosimetry |
| SEM | Scanning Electron Microscopy |
| SG | Structural-Geotechnical |
| UCS | Uniaxial Compressive Strength |
| WP | Work Package |

# Table of Contents

## Executive Summary

The knowledge of the decay of cultural heritage and prediction of the future risk to its survival are bound to the constituent materials, their properties, and the way they interact with the environment and respond to environmental stresses. From this perspective, Deliverable 4.2 collects and presents information on a series of building materials used in Europe, intended to feed decay and vulnerability models related to the conservation of cultural heritage.

The selected building materials include stones, bricks, and rammed heart from Italy, Greece, Spain, Norway, and Croatia, known for their historical usage or commercial value. These materials were investigated in the laboratory with a petrographic and physical-mechanical approach, encompassing a series of properties and characteristics involving material texture, colour, density, porosity, hydric and thermal behaviour, strength, deformability, and resistance to artificial accelerated weathering by salt crystallization and freezing-thawing. These represent some of the most significant parameters affecting material deterioration.

The properties of the different building materials are here presented in datasets and representative plots, often stressing the differences in performance connected with diverse compositions, or lithogenesis, or manufacturing processes. In this way, valuable indications about the quality, durability and suitability of application of each material are provided.

# 1. Introduction

## 1.1 Background

The deliverable D4.2 collects and presents information on the properties of building materials investigated at UNIPD, with the collaboration of IUAV and UGR, after a selection planned among all Hyperion partners directly related to Work Package (WP) 4. The contents of this deliverable refer to Tasks 4.1 and 4.3 of WP4 and are integrated by the deliverable D4.1 edited by IUAV (sharing Task 4.1). The dataset presented will feed the models created within HYPERION simulating the decay and vulnerability of cultural heritage in Europe. These models are part of the Hygro-Thermal (HT) and Structural-Geotechnical (SG) simulation tools, in the framework of the Holistic Risk Assessment Platform (HRAP) (Figure 1).

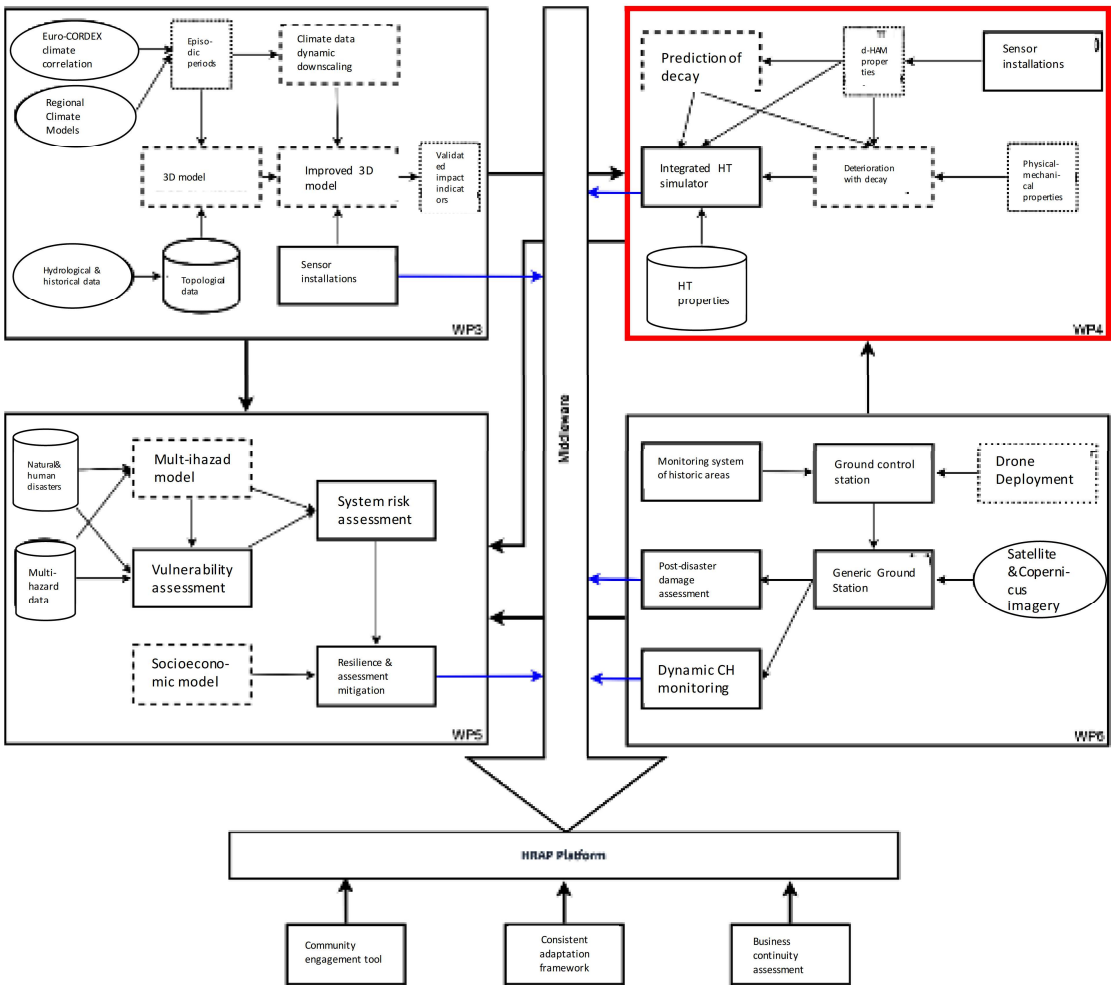


Figure 2: WP4 setting marked in red within the HYPERION's framework, as defined in D2.3.

## 1.2 Purpose and scope

The research described in D4.2 aims at providing a comprehensive characterization of selected types of stones, bricks, and rammed earth used in the built heritage, particularly of their texture and physical-mechanical properties. The focus is on the main properties affecting the decay and vulnerability of heritage materials, involving the way they behave when interacting with the environment and in response to environmental stresses. This study also provides data on the weathering patterns and kinetics as they change depending on the material.

Finally, this deliverable provides a reference for both Hyperion partners and any scholar/institution/body wishing to understand the past deterioration and predict the future risk of cultural assets made of the same (or similar) materials discussed here.

## 1.3 Approach

Firstly, the stones, bricks, and rammed earth investigated were selected and sampled in order to cover an array of diverse compositional and textural characteristics and based on their utilization in cultural heritage in different environments, including the HYPERION'S Tier buildings. Subsequently, the selected materials were prepared (cut, shaped, ground, etc.) for a series of analyses and tests conducted in the laboratory. They were run following a scheme of basic petrographic and physical-mechanical characterization completed by cycles of artificial accelerated weathering. The following properties or characteristics were studied:

- texture;
- colour;
- bulk and matrix density;
- open porosity and pore-size distribution;
- hydric properties, i.e., capillary water absorption, unforced/forced water absorption, water content;
- thermal properties, i.e., thermal conductivity, heat capacity, and thermal diffusivity;
- mechanical strength and deformability, i.e., uniaxial compressive strength (UCS), Young's modulus, and Poisson's ratio;
- ultrasound wave propagation and related indirect properties;
- resistance to salt crystallization;
- resistance to freeze-thaw.

# 2. Materials and methods

## 2.1 Selection

### *Stone*

The stone materials were sampled in different locations in Italy, Greece, Spain, Norway, and Croatia, and comprise mostly carbonate rocks, which are often the most susceptible of chemical alteration due to weathering and may present a wide variety of petrographic characteristics (Table 1, Figure 2, and Figure 3).

Table 2: List of the stones investigated.

| Country | Stone name | Provision | Rock type | ID |
|---|---|---|---|---|
| Italy | Botticino | Nordexplo' SRL | Limestone (sedimentary) | BL |
| | Carrara marble | Nordexplo' SRL | Marble (metamorphic) | CM |
| | Costozza stone | Nordexplo' SRL | Limestone (sedimentary) | CS |
| | Euganean trachyte | Nordexplo' SRL | Trachyte (volcanic) | ETR |
| | Red Verona | Nordexplo' SRL | Limestone (sedimentary) | RV |
| Greece | Lartios stone | Petrodiaskosmitiky Kyriazis Bross | Sandstone (sedimentary) | LS |
| | Sfouggaria | Petrodiaskosmitiky Kyriazis Bross | Limestone (sedimentary) | SS |
| Spain | Macael marble | Tesela | Marble (metamorphic) | MM |
| | Santa Pudia | Tesela | Limestone (sedimentary) | GSP |
| Norway | Tønsberg latite | Oslo University | Latite (volcanic) | TRH |
| | Tønsbergite | Oslo University | Monzonite (intrusive) | TSY |
| Croatia | Istria stone | Nordexplo' SRL | Limestone (sedimentary) | IS |

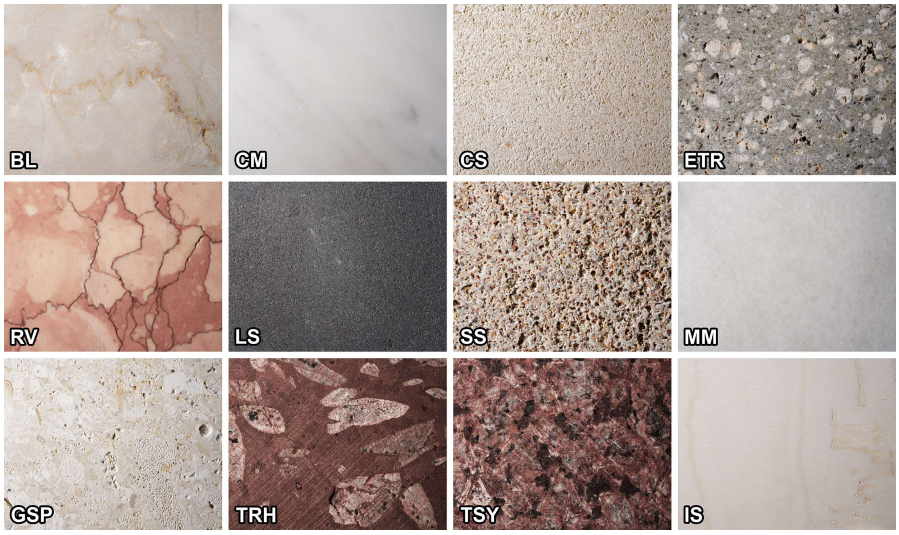


Figure 2: Photos of the stones investigated marked by their IDs (short side = 4 cm).

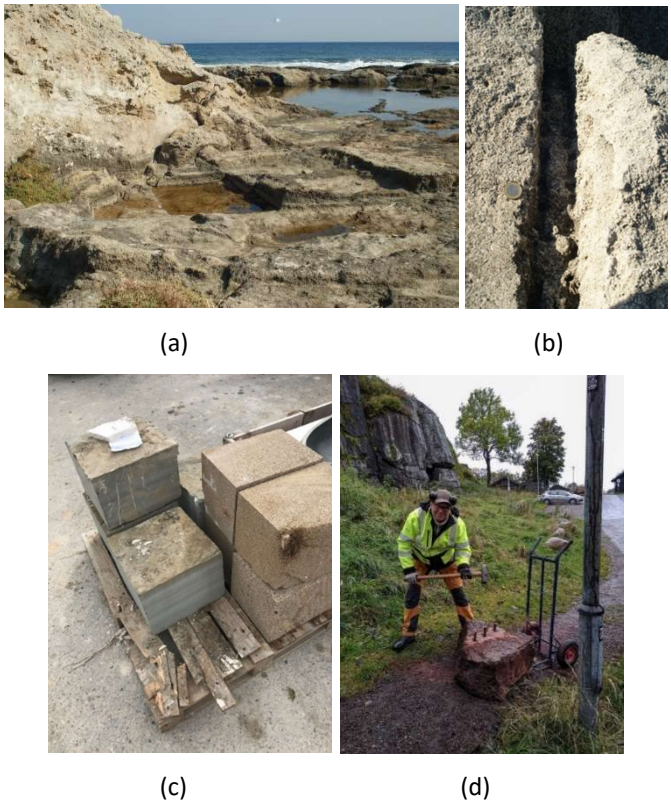

(a) (b)

(c) (d)

Figure 3: Sample collection. a) Survey at an ancient quarry in Rhodes, November 2019; b) Quarry marks in the ancient quarry; c) Sample prepared by the Petrodiaskosmitiky Kyriazis Bross (Rhodes); d) Sample collection in Norway by the colleagues of Oslo University.

### *Bricks*

Four types of commercial bricks (GP, RSS, RS, and R6) used in restoration of historic buildings were sampled in order to assess their aesthetic compatibility with the historic Venetian brick masonries. These bricks (Figure 4) are produced by the "soft mud" method and fired at the following temperatures: GP (yellow coloured) at 1050°C; RSS and R6 (red coloured) at 950 and 600°C, respectively; RS (pink coloured) at 980°C.

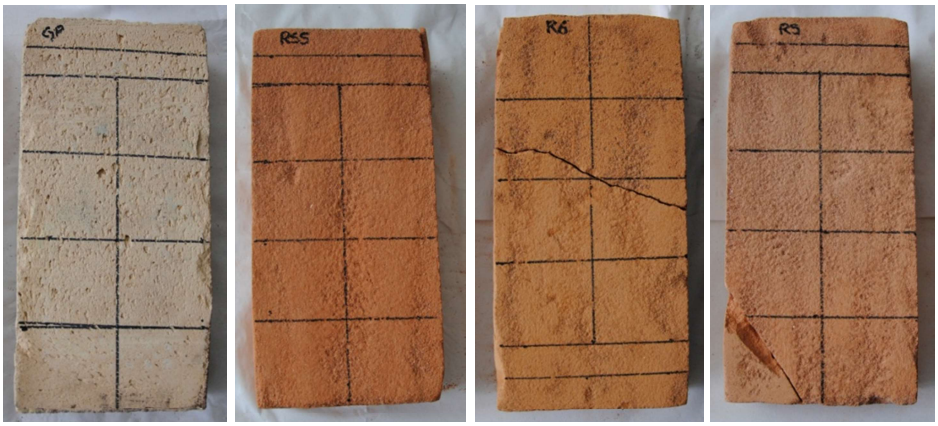


Figure 4: Photos of the bricks investigated marked by their IDs.

### *Rammed earth*

Rammed earth samples were collected in a quarry located 45 km from the city of Granada (Spain). The earth material was hand-mixed with the optimum water content (8% by mass) and a cylindrical mould was used to prepare the specimens. The mould has a diameter of 15 cm and a height of 30 cm. There were six compaction layers in each specimen, with 2 kg of earth material. The Proctor Energy (E = 0.583 J/cm$^3$) was measured with a manual rammer and each compaction layer had a thickness of about 5 cm. In Figure 5 the preparation of the rammed earth specimens is presented.

(a) (b)

Figure 5: Preparation of the rammed earth specimens.

## 2.1 Analysis and testing

The selected materials were analysed and tested with the following techniques and methods in the laboratories of UNIPD, except where indicated otherwise.

Texture was observed and characterized on samples prepared as 30 µm thin sections under the polarized-light microscope (IUAV); and by Scanning Electron Microscopy (SEM) with a CamScan MX-2500 microscope equipped with a $LaB_6$ cathode and operating at 20 kV and 160 nA, coupled with an EDS Sapphire Si(Li) detector (LEAP+Si(Li) crystal). As for the earth samples, grain size distribution was obtained by sieving (for elements > 0.063 mm) following EN ISO 17892-4:2019 (UGR).

Color was assayed on a 3nh spectrophotometer according to the CIELab system. The degree of color difference (ΔE*) was calculated according to the following equation:

$$\Delta E = \sqrt{(L^*_2 - L^*_1)^2 + (a^*_2 - a^*_1)^2 + (b^*_2 - b^*_1)^2}$$

where subscript ‘1’ refers to measurements on dry samples and subscript ‘2’ on wet samples. Measurements were carried out under a CIE standard illuminant D65 (simulating daylight with a color temperature of 6504 K) with SCI/SCE modes and wavelengths between 400 and 700 nm.

Bulk density was measured according to the standard EN 1936:2006, and also by mercury intrusion porosimetry (MIP), as reported below.

Open porosity and pore-size distribution were measured by MIP, with a porosimeter Thermo Scientific Pascal 140-240, covering a pore-radius range of 0.003–100 µm, on samples having a volume of about 1.5 $cm^3$. Complementary calculations of bulk and matrix density were also done (IUAV).

Capillary water absorption was determined according to the standard EN 15801:2009 (IUAV) and unforced/forced water absorption according to UNI EN 1925:2000. Moreover, water content for optimum compaction was determined with the Standard Proctor test, according to UNE 103-500-94 (UGR).

Thermal conductivity, heat capacity, and thermal diffusivity were measured with a portable device Applied Precision Isomet 2114, using the transient line source method (Kušnerová et al. 2013), having an accuracy of about 5% for thermal conductivity.

UCS, tangent Young's modulus, and tangent Poisson's ratio of the stones were measured according to the standard ASTM D7012-14, applying a stress rate of 1 MPa/s and recording the strains with strain gauges by Tokyo Measuring Instruments Lab. (three 30 mm axial sensors and one 90 mm transverse sensor per specimen). For the earth specimens, instead, linear transducers LVDT with a range of 10 mm were used to measure axial deformations, and creep tests were carried out introducing a uniaxial constant load until the stabilization of the readings in time was observed (UGR).

Ultrasound wave propagation was measured with an EPOCH650® Ultrasonic Flaw Detector (Olympus) by the direct transmission method (standard EN 14579:2004) recording p-wave and s-wave velocity along three orthogonal axes for each specimen. Complementary calculations of Young's modulus, Poisson's ratio, shear modulus, and bulk modulus were also done.

Resistance to salt crystallization was evaluated through an experimental program of 100 cycles of salt attack, each cycle consisting of: 2 h total immersion in a 14% $Na_2SO_4$ aqueous solution, minimum 16 h drying at 105 °C, and 2 h cooling (standard EN 12370:1999); the macroscopic deterioration and changes of mass and p-wave and s-wave velocity were monitored during the program.

The same experimental outline was followed for assessing resistance to freezing-thawing, but each of the 100 freeze-thaw cycles consisted of one freezing phase in air (6 h at –20 °C) and one thawing phase in water (6 h total immersion in water at room temperature); the specimens subjected to this program were initially water saturated (standard EN 12371:2001).

# 3. Stone

## 3.1 Texture

The selected stones can be classified in five texture groups listed and described in Table  and showed in Table 3.

Table 2: List and description of the texture groups classifying the selected stones.

| Texture group | Description | Grain size | ID |
|---|---|---|---|
| Micritic | Mainly micritic (<4 μm) made of very fine-grained crystals (calcite). Rarely some veins of coarser-grain size calcite are present. | <4 μm | BL |
| | | | RV |
| | | | IS |
| Sparitic/Micritic | Coexistence of micritic (<4 μm) and sparitic grain size both in fossils fillings (F) (mud or cement) or as binder (B) (matrix or cement). | Micritic (F) Sparitic (F+B) | CS |
| | | Micritic (F) Sparitic (B+clasts) | LS |
| | | Micritic (F) Sparitic (F+B) | SS |
| | | Micritic (B) Sparitic (F) | GSP |
| Crystalline granofelsic | Holocrystaline, heteroblastic, mosaic-like, sometimes with 120° triple junctions. | 0,1-0,7 mm | CM |
| | | 0,3-1,6 mm | MM |
| Porphyritic | Aphanitic with phenocrysts (Phc) fluctuating in a microcrystalline or partially vitreous groundmass | 1-6 mm (Phc) | ETR |
| | | 5-30 mm (Phc) | TRY |
| Holocrystalline | Phanerocrystalline, holocrystalline, equigranular, hypidiomorphic, coarse-grained. | 5-10 mm | TSY |

Table 3: Representative thin-section photomicrographs illustrating the different texture groups.

| Texture group | Photomicrograph |
|---|---|
| Micritic<br>BL (crossed-polarized light) | 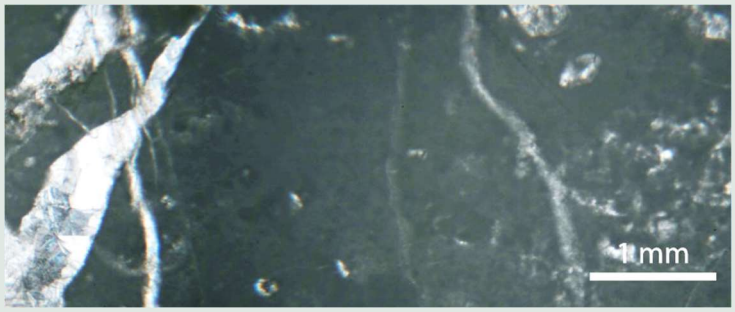 |
| Sparitic/Micritic<br>CS (plane-polarized light) | 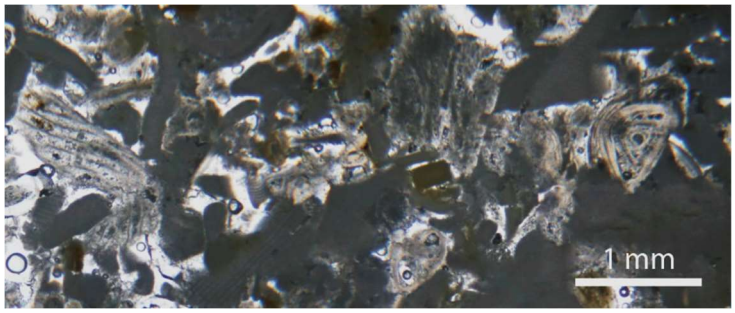 |
| Crystalline granofelsic<br>CM (crossed-polarized light) | 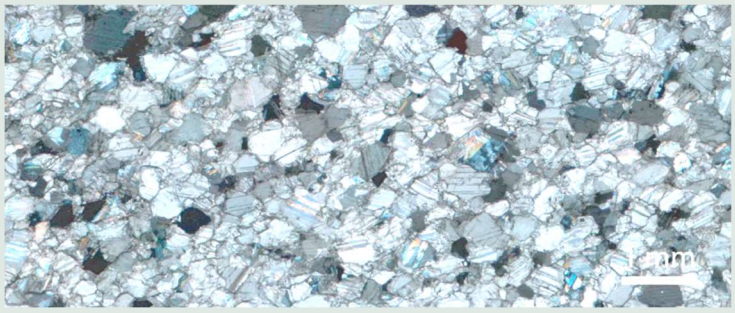 |
| Porphyrytic<br>TRH (crossed polarized light) | 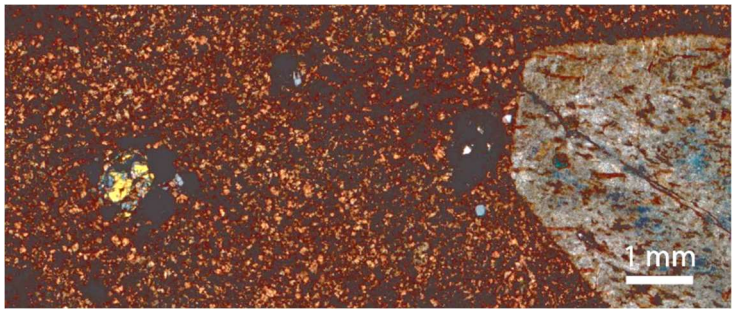 |
| Holocrystaline<br>TSY (crossed polarized light) | 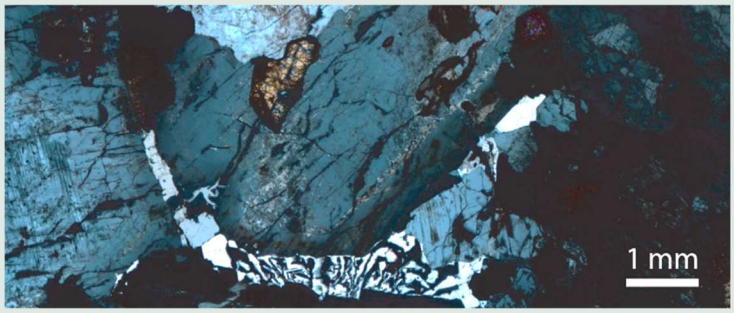 |

## 3.2 Physical properties

Table 4 to 7 gather the measures of petrophysical properties of the selected building stones.

Two main groups can be recognized. The first includes most of the materials, being dense, having an open porosity lower than about 1% and diverse composition. The second includes only limestones, namely CS, SS, and GSP, having a bulk density lower than 2 g/cm$^3$ and a high porosity, from 17% to 29% on average. In between, stands the volcanic rock ETR.

On the other hand, the pore-size distributions (Figure 6 shows an example) are more changing and make the petrophysical classification more complex. They can support the interpretation of the measures of water absorption, since the movement of liquid water is favoured when capillary pores (that is, 0.1 to 1000 μm of diameter, Klopfer 1985) prevail over the smaller micropores. The amount of absorbed water is also dependent on the volumetric percentage of porosity.

The most porous stones are associated with the worst thermal performance, as pointed about by the lower values of conductivity and the other thermal properties.

Table 4: Density measures (g/cm$^3$) obtained with different methods.

| | BL | CM | CS | ETR | RV | LS | SS | MM | GSP | TRH | TSY | IS |
|---|---|---|---|---|---|---|---|---|---|---|---|---|
| **Bulk density (EN 1936)** | 2.68 | 2.66 | 1.90 | 2.42 | 2.66 | 2.59 | 1.89 | 2.69 | 1.80 | 2.60 | 2.64 | 2.66 |
| **Bulk density (MIP)** | 2.74 | 2.71 | 1.97 | 2.45 | 2.69 | 2.67 | 2.25 | 2.72 | 2.21 | 2.65 | 2.72 | 2.71 |
| **Matrix density (MIP)** | 2.75 | 2.72 | 2.75 | 2.65 | 2.69 | 2.7 | 2.71 | 2.73 | 2.75 | 2.67 | 2.73 | 2.71 |

Table 5: Open porosity (vol%) and pore-size distribution (expressed as % of three pore-radius classes) determined by MIP.

| | | BL | CM | CS | ETR | RV | LS | SS | MM | GSP | TRH | TSY | IS |
|---|---|---|---|---|---|---|---|---|---|---|---|---|---|
| **Open porosity** | | 0.29 | 0.46 | 28.60 | 7.66 | 0.08 | 1.06 | 17.04 | 0.41 | 19.65 | 0.82 | 0.43 | 0.09 |
| **Pore-size distribution** | **100–10 μm** | 7.0 | 8.4 | 19.8 | 1.2 | 29.8 | 3.3 | 55.2 | 14.1 | 1.0 | 13.7 | 6.6 | 35.1 |
| | **10–1 μm** | 12.2 | 4.6 | 35.4 | 5.8 | 24.6 | 2.3 | 17.2 | 19.5 | 13.3 | 7.5 | 5.5 | 20.9 |
| | **<1 μm** | 80.8 | 87.0 | 44.9 | 93.0 | 45.6 | 94.4 | 27.5 | 66.4 | 85.7 | 78.8 | 87.9 | 44.0 |

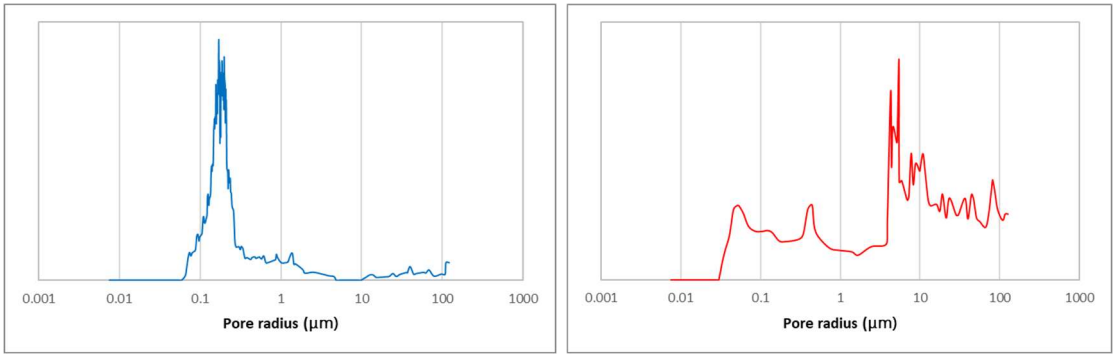


Figure 6: Representative curves showing the different pore-size distributions of CM (in blue) and RV (in red).

Table 6: Water absorption coefficient by capillarity (W, $g/m^2 \cdot s^{0.5}$) with standard deviation.

| | BL | CM | CS | ETR | RV | LS | SS | MM | GSP | TRh | TSy | IS |
|---|---|---|---|---|---|---|---|---|---|---|---|---|
| W | 0.23 | 0.27 | 10.71 | 1.64 | 0.42 | 12.41 | 15.26 | 0.18 | 16.5 | 0.86 | 0.58 | 0.33 |
| SD | 0.16 | 0.02 | 2.77 | 0.16 | 0.12 | 1.45 | 1.8 | 0.01 | 2.17 | 0.24 | 0.03 | 0.23 |

Table 7: Measures of thermal conductivity (λ, W/mK), heat capacity (C, $MJ/m^3 \cdot K$), and thermal diffusivity (α, $m^2/s$).

| | BL | CM | CS | ETR | RV | LS | SS | MM | GSP | TRH | TSY | IS |
|---|---|---|---|---|---|---|---|---|---|---|---|---|
| λ | 3.05 | 2.52 | 1.30 | 1.54 | 2.82 | 2.97 | 1.26 | 2.45 | 1.51 | 1.93 | 1.76 | 2.97 |
| C | 2.14 | 1.83 | 1.67 | 1.81 | 1.99 | 2.02 | 1.62 | 1.78 | 1.73 | 1.84 | 1.71 | 1.99 |
| α | 1.42 | 1.38 | 0.78 | 0.85 | 1.42 | 1.46 | 0.78 | 1.37 | 0.87 | 1.05 | 1.03 | 1.49 |

## 3.3 Mechanical properties

Table 8 shows the characteristics of mechanical strength and deformability of the selected building stones. Most of the materials investigated have a good to very good mechanical performance, with UCS values generally higher than 100 MPa (even exceeding 150 MPa in some cases). Three stones, namely CS, SS, and GSP are quite weak, with UCS ranging between 10 and 22 MPa on average, and Young's modulus comprised between 13 and 17 GPa; these also showed the highest porosity values during the petrophysical tests, as mentioned previously. A comparison of the stress-strain curves of a strong and a weak stone material from those two groups is proposed in Figure 7. LS and MM, instead, have intermediate UCS values, around 80 MPa. Poisson's ratio, instead, shows less significant trends for discriminating the different stone varieties.

Table 8: UCS (MPa), tangent Young's modulus (E, GPa), and Poisson's ratio (v, -) with standard deviations in parentheses.

| | BL | CM | CS | ETR | RV | LS | SS | MM | GSP | TRH | TSY | IS |
|---|---|---|---|---|---|---|---|---|---|---|---|---|
| UCS | 140.75 (±16.54) | 129.15 (±13.1) | 22.27 (±8.76) | 130.86 (±5.83) | 115.22 (±22.31) | 82.36 (±37.58) | 13.46 (±8.94) | 76.74 (±6.74) | 9.51 (±3.47) | 140.95 (±15.67) | 117.86 (±8.56) | 106.89 (±43.56) |
| E | 77.21 (±3.13) | 70.15 (±4.19) | 16.27 (±2.95) | 33.27 (±1.03) | 67.02 (±1.71) | 34.25 (±12.66) | 17.09 (±6.97) | 49.09 (±6.38) | 13.12 (±3.17) | 59.09 (±2.42) | 59.79 (±3.58) | 69.74 (±4.4) |
| v | 0.30 (±0.01) | 0.30 (±0.02) | 0.25 (±0.08) | 0.29 (±0.02) | 0.34 (±0.08) | 0.19 (±0.05) | 0.26 (±0.07) | 0.25 (±0.1) | 0.26 (±0.13) | 0.27 (±0.03) | 0.34 (±0.07) | 0.35 (±0.08) |

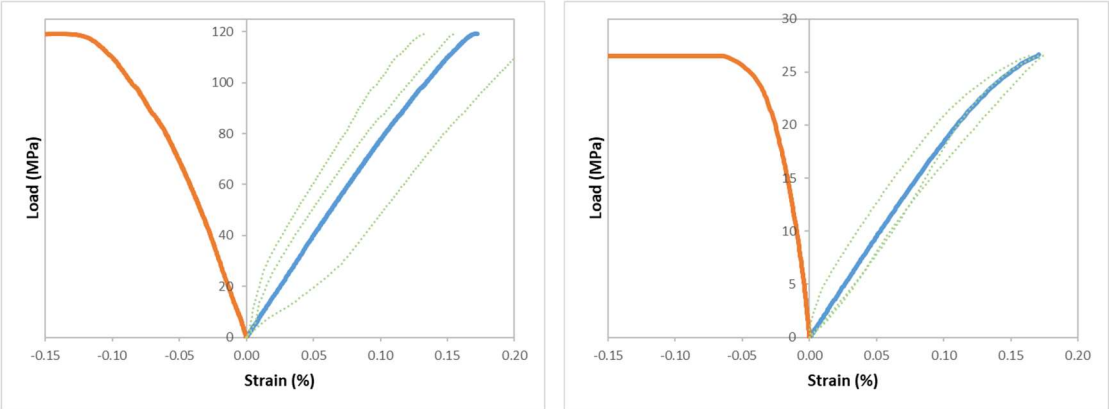


Figure 7: Representative stress-strain curves of BL (left) and CS (right) up to specimen break. The positive x-axis indicates axial strains (green dotted lines from each of the three strain gauges and solid blue lines from the averages) and the negative x-axis indicates transverse strains (orange lines).

Table 9: Summary of the ultrasound measurements: p-wave velocity ($v_p$, km/s), s-wave velocity ($v_s$, km/s), total and relative anisotropy of ultrasound velocity (ΔM and Δm, -), together with the indirect measures of Young's modulus (E, GPa), Poisson's ratio (v, -), shear modulus (G, GPa), and bulk modulus (K, GPa).

| | BL | CM | CS | ETR | RV | LS | SS | MM | GSP | TRH | TSY | IS |
|---|---|---|---|---|---|---|---|---|---|---|---|---|
| $v_p$ | 6.63 | 5.58 | 3.32 | 4.37 | 6.29 | 4.98 | 3.72 | 4.47 | 3.35 | 5.57 | 5.03 | 6.42 |
| $v_s$ | 3.16 | 2.89 | 1.83 | 2.38 | 3.00 | 2.82 | 2.04 | 2.40 | 1.75 | 2.82 | 2.72 | 3.06 |
| ΔM | 1 | 5 | 6 | 2 | 4 | 12 | 2 | 22 | 8 | 5 | 2 | 1 |
| Δm | 1 | 4 | 4 | 2 | 3 | 8 | 2 | 1 | 4 | 2 | 1 | 1 |
| E | 74.65 | 60.48 | 20.00 | 36.23 | 66.51 | 54.50 | 24.26 | 41.16 | 18.80 | 36.23 | 52.87 | 69.66 |
| v | 0.35 | 0.32 | 0.28 | 0.29 | 0.35 | 0.26 | 0.29 | 0.30 | 0.31 | 0.29 | 0.29 | 0.35 |
| G | 27.72 | 22.98 | 7.80 | 14.06 | 24.59 | 21.59 | 9.43 | 15.86 | 7.17 | 14.06 | 20.45 | 25.75 |
| K | 81.11 | 54.68 | 15.30 | 28.56 | 75.16 | 38.20 | 18.89 | 33.84 | 16.64 | 28.56 | 42.53 | 78.73 |

The results of the ultrasound measurements can be considered a synthesis of the findings of the physical-mechanical tests described so far (Table 9). The propagation velocity of ultrasound waves, in fact, is dependent on the characteristics of density/porosity and deformability of the materials through which they travel. Therefore, it is not surprising that the most porous and softest stone varieties register the lowest values – around 3.5 km/s for p-waves and 2 km/s for s-waves. The indirect calculation of deformability parameters, in some cases, also allowed a validation of the same properties directly measured and discussed above, showing a good correlation.

## 3.4 Artificial accelerated weathering

The salt crystallization and freeze-thaw tests highlighted a good durability of the stones under environmental stresses. The curves of weight variation after salt crystallization (Figure 8) and freeze-thaw test (Figure 9) display similar behaviour for most samples, except for the most porous rocks, i.e., CS, GSP, and SS. Damage after accelerated ageing tests is visually limited and localized principally to edges and corners of the cubic samples or, where present, along stylolites. The decay of LS is characterized by the detachment of lamellar slices from the cube's sides, whereas MM is affected by a progressive sugaring, creating a very granulated surface appearance.

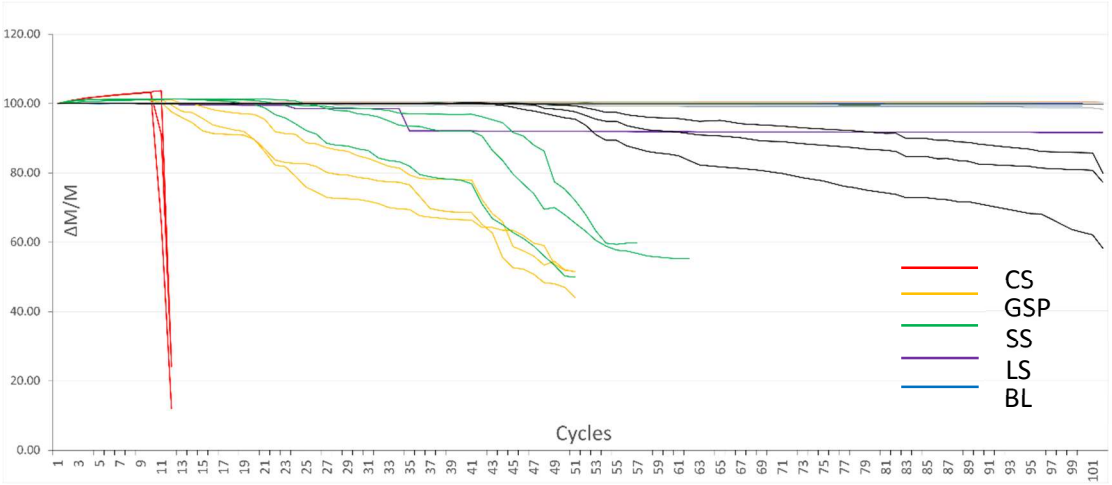


Figure 8: Weight variation (ΔM/M) of the stones during 100 salt-crystallization cycles.

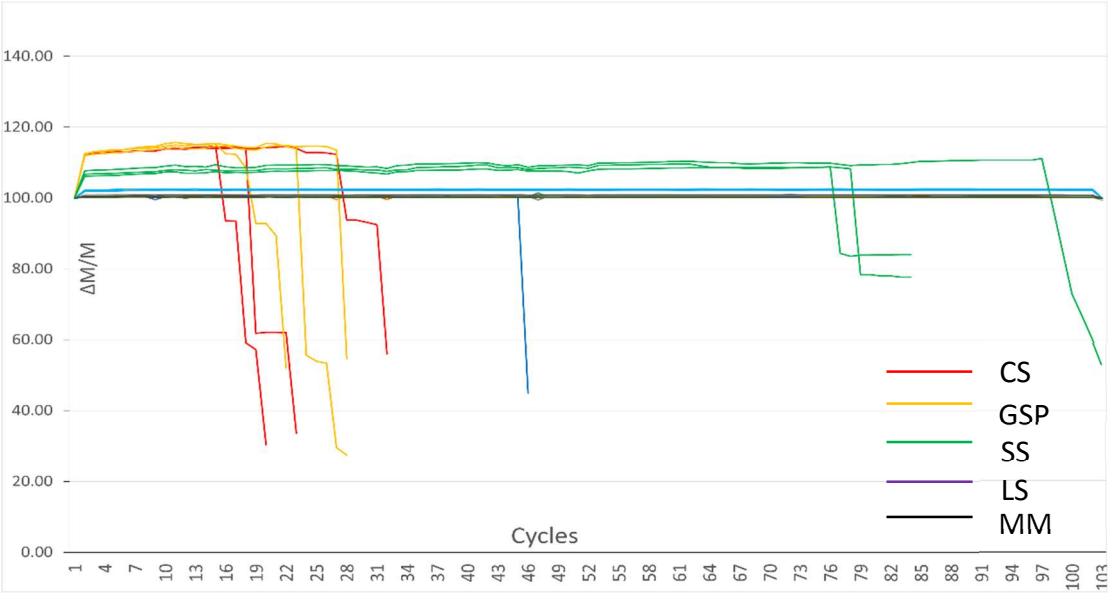


Figure 9: Weight variation (ΔM/M) of the stones during 100 freeze-thaw cycles.

In order to evaluate the evolution of the damage effects of salt and ice in the pore system, $V_p$ values were measured at regular steps (every 10 cycles) during the ageing tests. The results follow the considerations reported about the weight loss curves: most samples show a similar trend, except for the weakest lithologies. The monitoring was very useful in order to detect internal cracks, not detectable just by the visual observation. This is evident when there is no wave transmission even before the visible stone damage. In these cases, microcracks and fissures develop, hindering wave transmission in the materials.

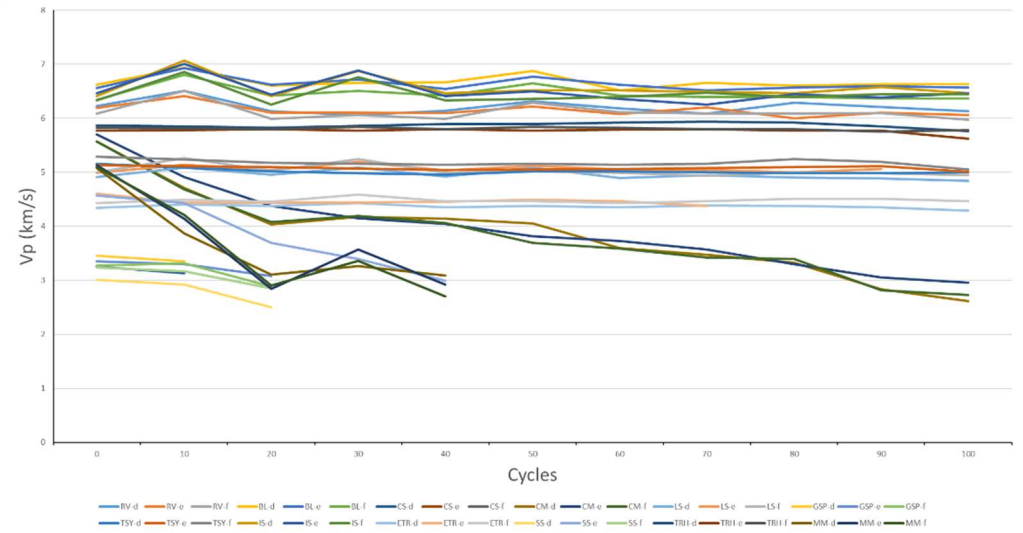


Figure 10: Propagation velocities of ultrasonic $V_p$ pulses (km/s) during salt crystallization test.

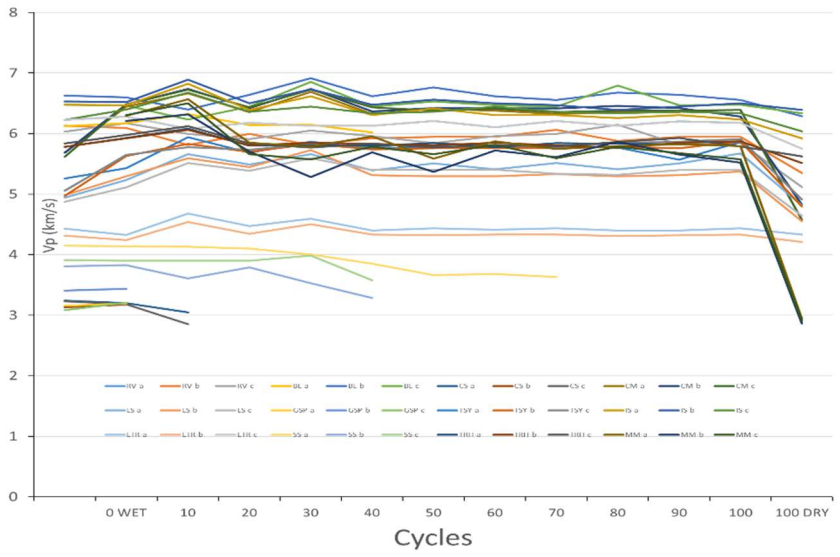


Figure 11: Propagation velocities of ultrasonic $V_p$ pulses (km/s) during freeze-thaw test.

More in detail, selected ultrasound results from specific lithologies are reported below, in order to better define their behaviour in presence of different environmental conditions.

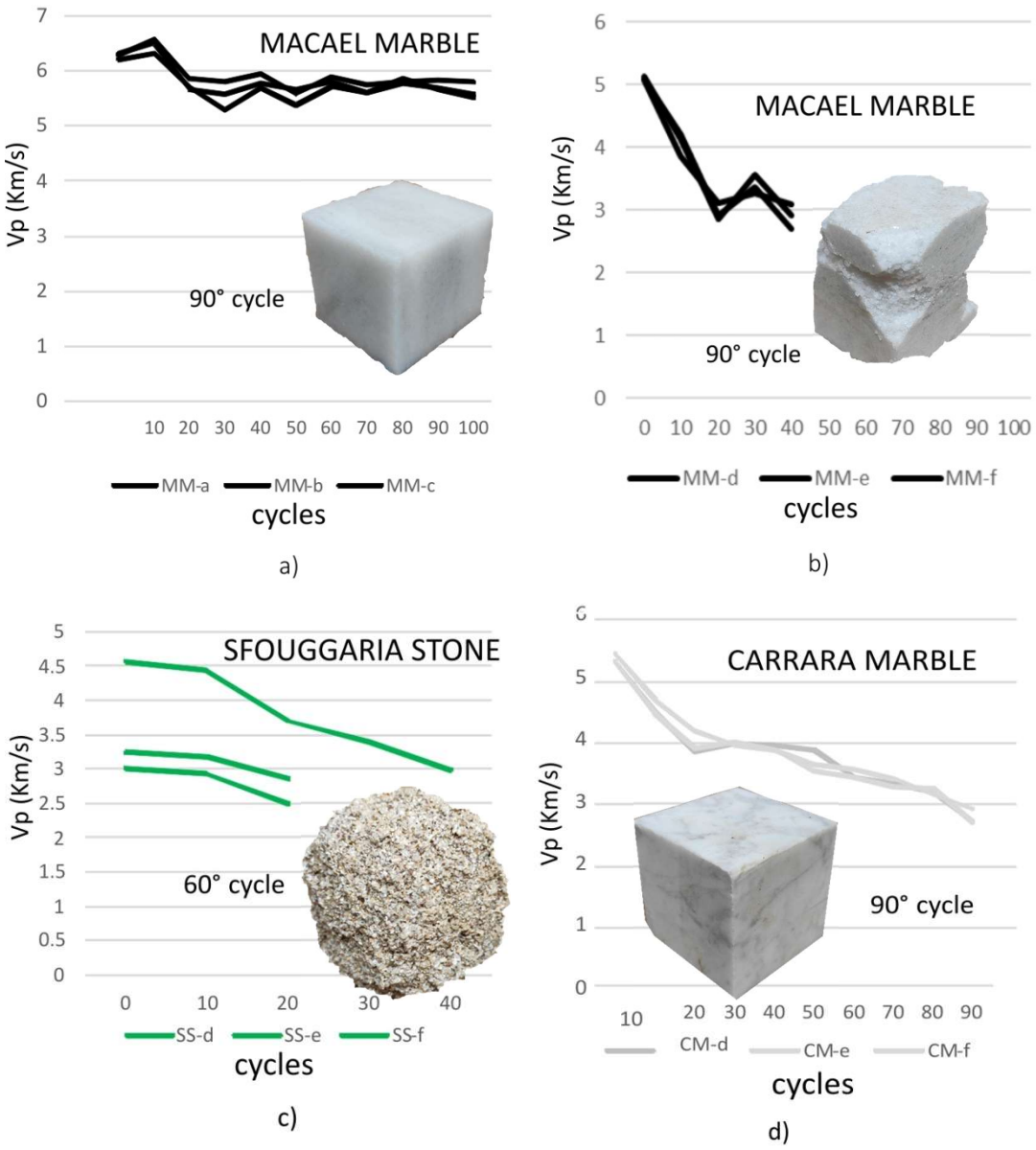


Figure 12: Ultrasound monitoring: a) Macael marble at 90°cycle under freeze-thaw test; b) Macael marble at 90°cycle under salt crystallization test; c) Sfouggaria stone at 60°cycle under freeze-thaw test; d) Carrara marble at 90°cycle under salt crystallization test.

At the end of the cycles, both $V_p$ and $V_s$ pulses were measured on the samples. The physical-mechanical parameters strongly decrease. Some increasing velocities during salt crystallization cycles are due to the precipitation of salts in the pores.

Table 10: Ultrasound test before and after the aging cycles. Propagation velocities of ultrasonic $V_p$ and $V_s$ pulses (m/s); E = Young's modulus (GPa); G = shear modulus (GPa); K = bulk modulus (GPa).

| | | BL | CM | CS | ETR | RV | LS | SS | MM | GSP | TRH | TSY | IS |
|---|---|---|---|---|---|---|---|---|---|---|---|---|---|
| Before aging cycles | $v_p$ | 6521 | 5577 | 3322 | 4370 | 6290 | 4976 | 3720 | 4469 | 3346 | 5569 | 5032 | 6416 |
| | $v_s$ | 3160 | 2895 | 1830 | 2383 | 3002 | 2825 | 2037 | 2400 | 1750 | 2815 | 2724 | 3062 |
| | E | 74.65 | 60.48 | 20 | 36.23 | 66.51 | 54.5 | 24.26 | 41.16 | 18.8 | 56.53 | 52.87 | 69.66 |
| | G | 27.72 | 22.98 | 7.8 | 14.06 | 24.59 | 21.59 | 9.43 | 15.86 | 7.17 | 21.28 | 20.45 | 25.75 |
| | K | 81.11 | 54.68 | 15.3 | 28.56 | 75.16 | 38.2 | 18.89 | 33.84 | 16.64 | 54.87 | 42.53 | 78.73 |
| After salt cycles | $v_p$ | 6367 | 2730 | - | 4467 | 5970 | 4943 | - | - | - | 5775 | 5049 | 6448 |
| | $v_s$ | 3073 | 1365 | - | 2369 | 2925 | 2526 | - | - | - | 2920 | 2648 | 3008 |
| | E | 70.69 | 13.63 | - | 36.26 | 62.66 | 45.69 | - | - | - | 60.8 | 50.65 | 67.65 |
| | G | 26.22 | 5.11 | - | 13.9 | 23.35 | 17.26 | - | - | - | 22.89 | 19.33 | 24.85 |
| | K | 77.59 | 13.63 | - | 30.88 | 66.13 | 43.08 | - | - | - | 59.01 | 44.5 | 81.07 |
| After freeze-thaw cycles | $v_p$ | 6312 | 4712 | - | 4268 | 5406 | 4670 | - | 2906 | - | 5621 | 4921 | 6115 |
| | $v_s$ | 3094 | 2586 | - | 2313 | 2760 | 2688 | - | 1923 | - | 2872 | 2601 | 2978 |
| | E | 71.33 | 47.13 | - | 34.24 | 55.03 | 48.96 | - | 22.62 | - | 58.6 | 48.71 | 65.51 |
| | G | 26.58 | 18.34 | - | 13.25 | 20.79 | 19.55 | - | 10.18 | - | 22.14 | 18.65 | 24.36 |
| | K | 75.18 | 36.45 | - | 27.44 | 52.03 | 32.94 | - | 9.68 | - | 55.29 | 41.89 | 70.23 |

# 4. Bricks

## 4.1 Texture

Microtexture and vitrification level were studied by both optical microscopy and scanning electron microscopy (SEM) on polished thin sections.

Under the optical microscope, bricks appeared texturally homogeneous (Figs. 13 a-d). Inclusions were predominant sub-rounded grains of quartz and feldspar, varying in size up to 1 mm. Porosity is generally vugh shaped.

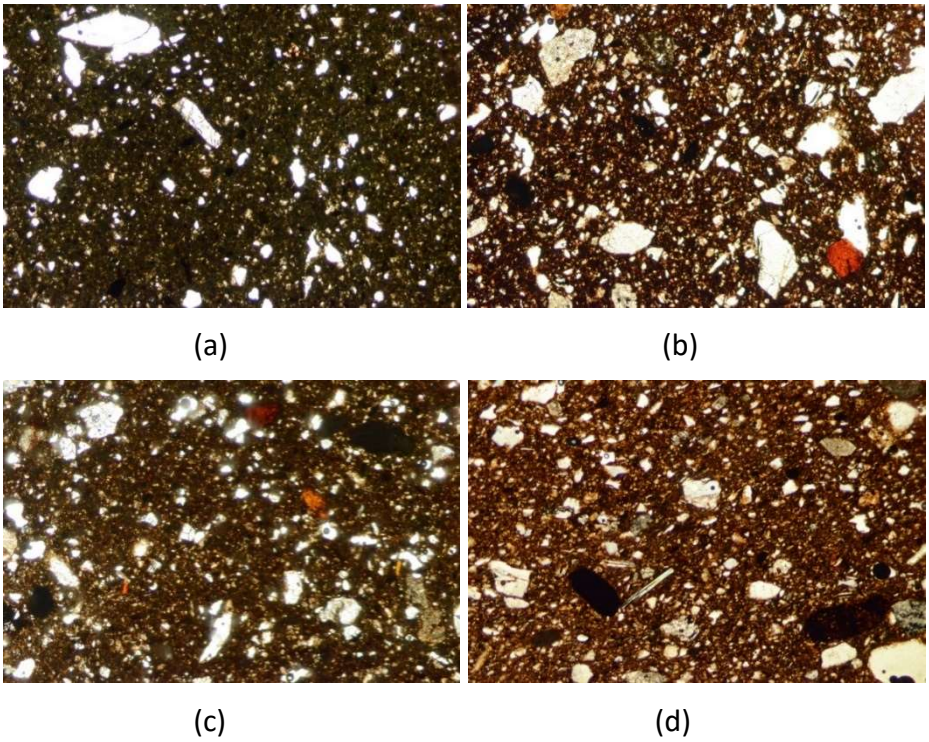


Figure 13: Photomicrographs (plane-polarized light) of the commercial bricks (3.2 X): a) brick GP; b) brick RSS; C) brick RS; d) brick R6.

SEM observations permit to see other textural details (Figs. 14 a-d). Phyllosilicates maintained their sheet-like fabric, although the loss of OH- groups revealed exfoliation along basal plans. Carbonates were still recognizable, but secondary porosity appeared, due to $CO_2$ release from the crystals. Firing-induced transformation of feldspars is evident along preferential lines, like twinning and cleavage plains and at the boundaries. No evidence of melting could be seen in the groundmass. In RS, fired at 980°C, dehydroxylation was more extensive than in R6 and showed pseudomorphs of phyllosilicates.

The samples fired at higher temperatures (GP, RSS, and RS) had larger pores (up to 300 µm, respectively), while R6, fired at a lower temperature, had smaller pores (up to 150 µm). That confirms the influence of firing on pore size, since pores tend to increase in size when vitrification occurs, which produces larger and more circular pores (Benavente et al. 2006).

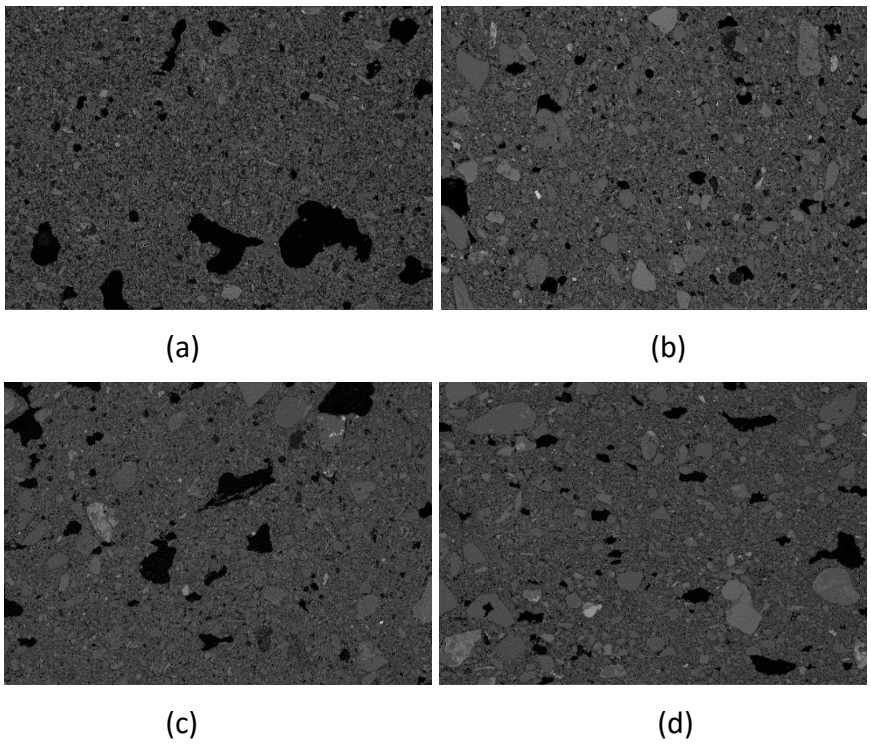


Figure 14: SEM-BSE images of fired commercial bricks: a) brick GP; b) brick RSS; C) brick RS; d) brick R6.

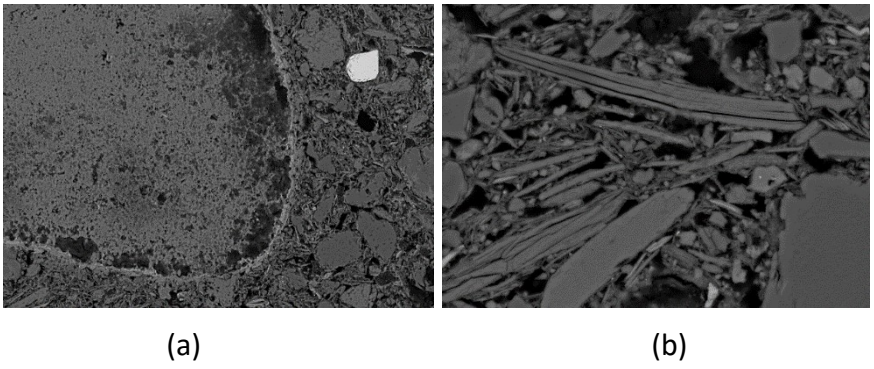


Figure 15: SEM-BSE images of the commercial bricks: a) calcite grain decomposition and secondary porosity, brick RS; b) phyllosilicates dehydroxylation along the 001 basal plans, brick R6.

## 4.2 Physical properties

Color changes in dry and wet samples were measured in order to verify esthetical qualities in different microclimate conditions (presence of rain and humidity). All samples show to be sensitive to color changes after wetting: in general a* and b* increase, while L* decreases (Table 11). The most sensitive bricks are the samples A3, A6, B2, B4, and C3, which show a color difference (ΔE) > 17. All the colour changes are outside the limit of perceptibility, defined as a ΔE ≥ 3 in the CIELAB color space (Benavente et al. 2002; Grossi et al. 2007), and therefore visible to the naked eye.

Table 11: Color coordinates, L*, a*, b* for commercial fired bricks, measured in dry and wet conditions and core (-c) and surface (-s) when differentiated. Also shown: color difference ΔE.

| | DRY | | | WET | | | |
|---|---|---|---|---|---|---|---|
| Sample | L* | a* | b* | L* | a* | b* | ΔE |
| A1 | 61.40 | 11.64 | 23.40 | 51.80 | 12.38 | 24.98 | 9.76 |
| A2 | 62.28 | 7.89 | 20.95 | 49.24 | 12.50 | 25.51 | 14.56 |
| A3 | 56.59 | 11.70 | 22.65 | 39.96 | 19.82 | 24.49 | 18.60 |
| A4 | 52.44 | 18.04 | 25.84 | 44.89 | 17.88 | 26.17 | 7.56 |
| A5 | 59.00 | 13.35 | 24.33 | 57.69 | 11.48 | 26.97 | 3.50 |
| A6 | 67.07 | 8.28 | 23.24 | 49.32 | 10.60 | 23.65 | 17.91 |
| A7 | 60.95 | 8.64 | 20.76 | 55.78 | 12.51 | 27.10 | 9.05 |
| A8 | 66.25 | 8.33 | 23.07 | 58.62 | 7.81 | 27.33 | 8.76 |
| A9 | 66.33 | 5.21 | 23.16 | 49.97 | 13.95 | 24.94 | 18.63 |
| A10 | 70.42 | 5.24 | 18.96 | 60.72 | 11.15 | 28.20 | 14.64 |
| A11 | 67.25 | 9.63 | 19.89 | 56.60 | 6.20 | 27.59 | 13.59 |
| A12 | 53.81 | 12.98 | 23.72 | 58.46 | 10.75 | 21.30 | 5.70 |
| A13 | 45.23 | 12.60 | 25.05 | 51.41 | 15.97 | 26.80 | 7.26 |
| B1 | 76.80 | 1.55 | 8.79 | 67.30 | 2.17 | 10.97 | 9.77 |
| B2 | 59.67 | 4.06 | 21.10 | 51.04 | 14.49 | 35.47 | 19.74 |
| B3 | 62.12 | 12.56 | 23.58 | 49.81 | 16.13 | 26.36 | 13.12 |
| B4 | 62.28 | 5.63 | 7.77 | 45.35 | 7.59 | 9.66 | 17.15 |
| B5 | 58.68 | 12.54 | 22.27 | 43.47 | 17.34 | 24.66 | 16.12 |
| B6 | 64.49 | 3.08 | 18.15 | 56.05 | 3.83 | 21.98 | 9.30 |
| B7 | 50.20 | 18.17 | 23.96 | 36.81 | 23.45 | 24.78 | 14.42 |
| B8 | 58.99 | 12.66 | 22.31 | 45.15 | 17.68 | 25.27 | 15.03 |
| B9 | 64.79 | 6.89 | 19.06 | 55.42 | 10.88 | 24.31 | 11.46 |
| B10 | 60.38 | 8.17 | 20.34 | 51.95 | 10.26 | 23.29 | 9.17 |
| B11-Y | 57.65 | 5.13 | 19.13 | 40.69 | 9.37 | 18.46 | 17.49 |
| B11-B | 36.65 | 3.40 | 9.15 | 28.10 | 4.88 | 11.14 | 8.90 |
| C1-W | 78.21 | -1.08 | 10.68 | 64.20 | -1.97 | 12.08 | 14.11 |
| C1-R | 68.81 | 7.82 | 21.34 | 56.44 | 11.73 | 26.55 | 13.98 |
| C2 | 63.74 | 2.36 | 27.99 | 55.08 | 3.03 | 33.42 | 10.25 |
| C3 | 61.13 | 8.16 | 15.05 | 41.31 | 16.04 | 20.55 | 22.03 |

Colorimetry allows to measure color variation in order to compare the aesthetic qualities to those of the original bricks of the Santa Maria dei Servi Church (Tier 2 building in Venice).

Samples R6 and RS show variations in color from the core (indicated by suffix –c) to the surface (indicated by suffix –s), due to non-homogeneous Fe oxidation of samples during firing. In particular, R6 shows a darker core than the outer sides; the opposite,

is found in RS, with a lighter core. Sample GP is the most sensitive to color changes after wetting, and both their a* and b* increase (Table 12).

Table 12: Color coordinates, L*, a*, b* for commercial fired bricks, measured in dry and wet conditions and core (-c) and surface (-s) when differentiated. Also shown: color difference ΔE.

| | L* | a* | b* | L* | a* | b* | ΔE |
|---|---|---|---|---|---|---|---|
| GP | 70.42 | 6.89 | 24.28 | 42.29 | 20.28 | 24.25 | 31.15 |
| RS-s | 60.23 | 16.41 | 25.86 | 46.77 | 17.75 | 24.94 | 13.56 |
| RS-c | 61.35 | 14.73 | 23.6 | - | - | - | - |
| RSS | 56.51 | 19.05 | 25.4 | 44.53 | 20.22 | 24.37 | 12.08 |
| R6-s | 54.79 | 14.92 | 25.58 | 38.85 | 17.19 | 22.82 | 16.34 |
| R6-c | 53.51 | 9.35 | 20.01 | 37.8 | 10.51 | 17.36 | - |

Concerning the water absorption behavior, GP was the brick with the highest free and forced absorption values (Ab = 27.63%, Af = 28.71%, respectively), RS and RSS showed intermediate values, whereas R6 stood out for its low capacity to absorb water (Ab = 17.36%, Af = 17.88%). GP had the lowest drying index (Di = 1.35) while R6 had the slowest (Di = 1.37) (Table 13). GP, the brick with the highest carbonate content, had the highest values of open porosity. The results of the capillarity test highlighted the trend followed by free water absorption. Sample GP had a capillarity rise of 0.43; R6 had the lowest value (Ks = 0.16); RS and RSS were intermediate.

Table 13: Hydric parameters: Ab = free water absorption (%); Af = forced water absorption (%); Drying index; $d_b$ = bulk density(kg/m$^3$); $D_{sk}$ = skeletal density (kg/m$^3$); Ks = capillarity coefficient; B = capillarity rise.

| | Hydric test | | | | | | | |
|---|---|---|---|---|---|---|---|---|
| | $A_b$ | $A_f$ | Di | p | $d_b$ | $d_{sk}$ | Ks | B |
| GP | 27.63 | 28.71 | 1.35 | 41.36 | 1.44 | 2.46 | 0.43 | 1.33 |
| RS | 22.6 | 23.09 | 1.36 | 36.75 | 1.58 | 2.5 | 0.32 | 1.21 |
| RSS | 21.57 | 23.28 | 1.37 | 37.52 | 1.61 | 2.57 | 0.3 | 1.29 |
| R6 | 17.36 | 17.88 | 1.37 | 31.14 | 1.72 | 2.5 | 0.16 | 0.72 |

## 4.3 Mechanical properties

The highest velocity values ($V_p$ and $V_s$) were measured in bricks GP (Table 14), and the lowest in R6, the former being the most compact bricks, and the latter the least. The highest total anisotropy value (ΔM) was observed in R6. Its low compactness and high anisotropy were in fact due to the absence or only incipient process of melting in the matrix and proved the presence of phyllosilicate sheets in the bulk, which produces preferential orientations, while at high temperature, as in GP, texture became more homogeneous. Poisson's ratio values were very similar in all the bricks.

Table 14: Physical mechanical parameters of commercial fired bricks. Hydric parameters: Ab = free water absorption (%); Af = forced water absorption (%);Di = drying index; p = open porosity; $D_b$ = apparent density (kg $m^{-3}$); $D_{sk}$ = real skeletal density (kg $m^{-3}$); Ks = capillarity coefficient; B = capillarity rise. Ultrasound test: propagation velocities of ultrasonic $V_p$ and $V_s$ pulses ($m/s^1$). ΔM = total anisotropy (%); v = Poisson's ratio; E = Young's modulus (GPa); G = shear modulus (GPa); K = bulk modulus (GPa).

| | Ultrasound test | | | | | | | |
|---|---|---|---|---|---|---|---|---|
| | $V_p$ | $V_s$ | ΔM | Δm | v | E | G | K |
| GP | 2773 | 1299 | 12.26 | 2.66 | 0.36 | 6.42 | 2.36 | 7.72 |
| RS | 2272 | 1106 | 14.26 | 1.59 | 0.34 | 3.31 | 1.12 | 3.67 |
| RSS | 1857 | 893 | 18.07 | 4.96 | 0.35 | 2.52 | 0.96 | 2.25 |
| R6 | 1441 | 752 | 20.38 | 0.91 | 0.31 | 3.31 | 1.23 | 3.67 |

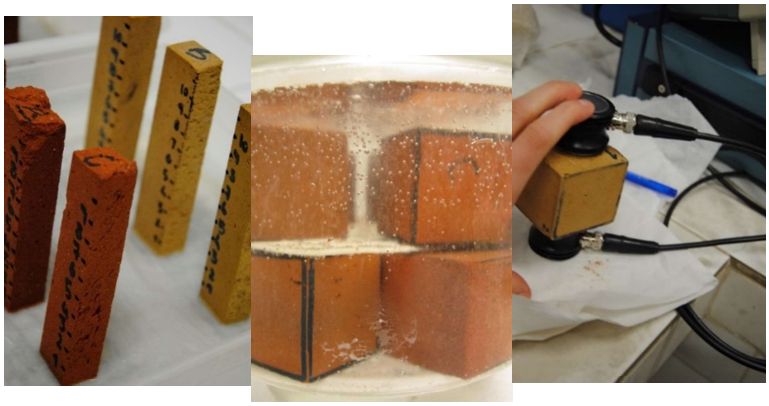

(a) (b) (c)

Figure 16: a) capillarity rise; b) forced water absorption; c) ultrasound test.

# 5. Rammed earth

## 5.1 Physical properties

The grain size distribution determined on the rammed earth specimens in showed in Figure 17.

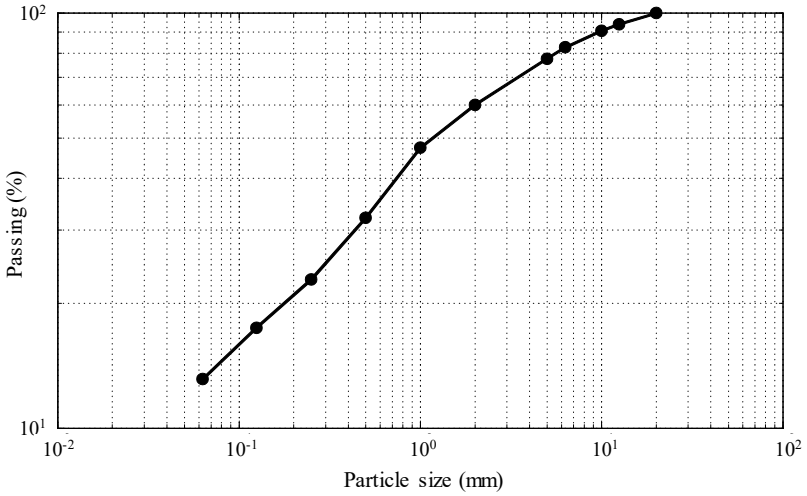


Figure 17: Particle size distribution (without the fine fraction).

Regarding the determination of the water content for optimum compaction, a range of 7% to 12% was selected to obtain the maximum dry density. It can be observed from Figure 18 that the optimum water content for preparation of rammed earth was 8% by mass.

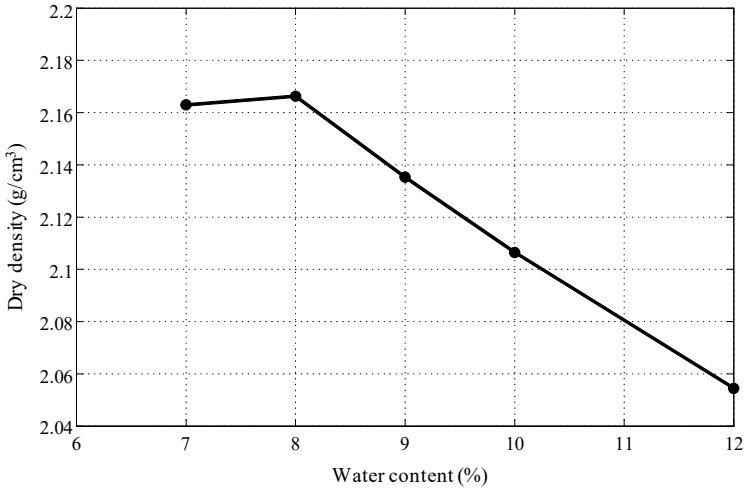


Figure 18: Results of the Standard Proctor test.

The samples were left drying for 4 months, however the moisture content variation with time shows a constant weight from the 25$^{th}$ day.

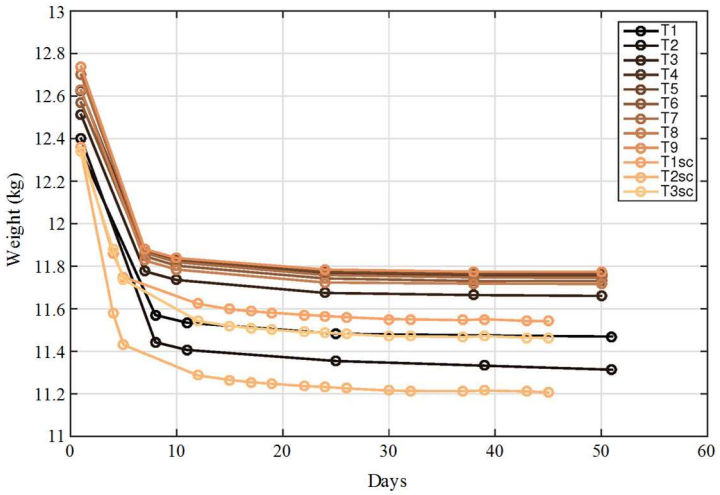


Figure 19: Moisture content variation with time.

## 5.2 Mechanical properties

The twelve samples tested under uniaxial compression (Figure 20 and 21) gave an average value of UCS of 0.74 ± 0.10 MPa and a Poisson's ratio of 0.206 ± 0.025.

Figure 20: Unconfined compressive strength test of rammed earth.

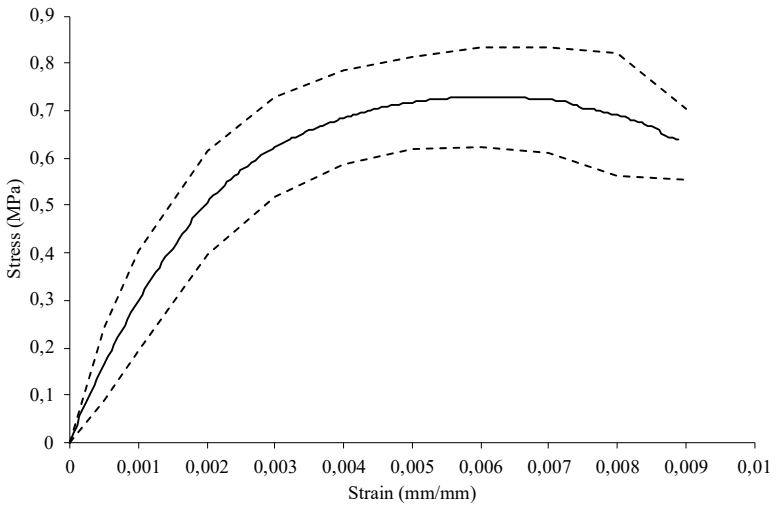


Figure 21: Average stress-strain curve of all the rammed earth samples tested (continuous black curve). Dashed black curves correspond to the standard deviation.

Six specimens were also tested under uniaxial compression at constant load, i.e., by creep tests (the load was introduced through a lever using a beam to transfer the load to each sample, Figure 22 and 23). The constant load value used in all the creep tests was determined by previous compression tests (10% of the compressive strength of the Proctor Test).

Figure 22: Configuration of the creep tests.

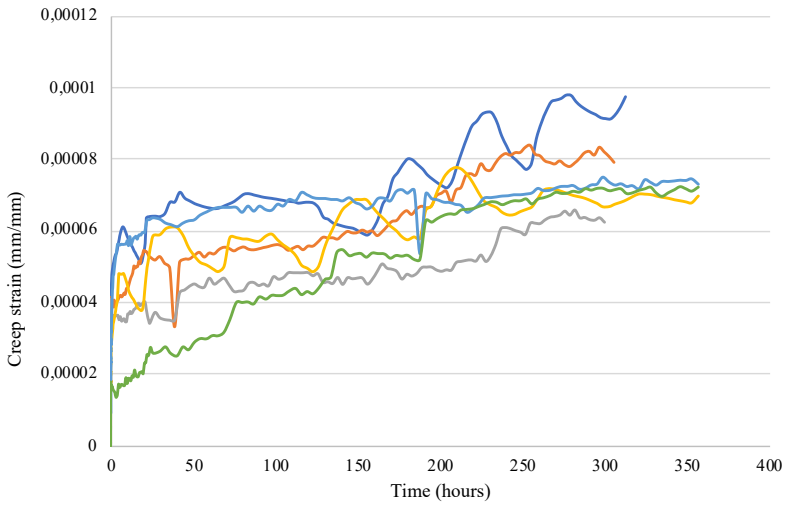


Figure 23: Experimental creep curves of the rammed earth tested samples.

# 6. CONCLUSIONS

Deliverable 4.2 presents the methods and results of a comprehensive laboratory characterization of building materials from Europe used in cultural heritage, discussing the textural, physical, and mechanical properties of selected stones, bricks, and rammed earth. The experimental phase was conducted in order to get information on critical properties affecting the decay of heritage materials and, indirectly, of cultural heritage. In fact, deterioration can be understood the best with a deep knowledge of the way the diverse composition and history of exploitation/manufacturing/application of geomaterials affect the conservation of heritage sites and structures where they are utilized.

The database contained in Deliverable 4.2 will support the completion of HYPERION's HRAP platform by providing numerical inputs for the HT and SG simulation tools, aimed at modelling and predicting the risk to cultural heritage brought about by environmental stresses and changes. This information will also possibly support the activities and decision-making protocols of the stakeholders interested in the preservation of cultural heritage and its vulnerability due to climate change.

Future developments of this study are planned, with the realization of advanced petrophysical measurements (not originally planned in the project, and made possible after the purchase of new instrumentation for material testing in controlled environmental conditions) and the interaction with the research carried out for the upcoming Deliverables 4.3, 4.4, and 4.5.

# 7. REFERENCES

1. ASTM D7012-14 (2014). Standard Test Methods for Compressive Strength and Elastic Moduli of Intact Rock Core Specimens under Varying States of Stress and Temperatures. West Conshohocken PA: ASTM.
2. Benavente D., Martiñez-Verdú F., Bernabeu A., Viqueira V., Fort R., García del Cura M.A., Illueca C., Ordóñez S. (2002). Influence of surface roughness on color changes in building stones. Color Research and Application, 28, pp. 343–351.
3. Benavente D., Linares-Fernández L., Cultrone G., Sebastián E. (2006) Influence of microstructure on the resistance to salt crystallisation damage in brick. Materials and Structures, 39, pp. 105–113.
4. EN 12370 (1999). Natural Stone Test Methods – Determination of Resistance to Salt Crystallisation. Brussels: CEN.
5. EN 12371 (2001). Natural Stone Test Methods – Determination of Frost Resistance. Brussels: CEN.
6. EN 14579 (2004). Natural Stone Test Methods – Determination of Sound Speed Propagation. Brussels: CEN.
7. EN 15801 (2009). Conservation of cultural property - Test methods - Determination of water absorption by capillarity. Brussels: CEN.
8. EN 1936 (2006). Natural stone test methods - Determination of real density and apparent density, and of total and open porosity. Brussels: CEN.
9. Grossi C.M., Brimblecombe P., Esbert R.M., Alonso F.J. (2007). Color changes in architectural limestones from pollution and cleaning. Color Research and Application, 32, pp. 320–331.
10. Klopfer H. (1985). Feuchte. In: Lutz P. et al., eds, Lehrbuch der Bauphysik. Teubner: Stuttgart, pp. 265–434.
11. Kušnerová M., Valíček J., Harničárová M., Hryniewicz T., Rokosz K., Palková Z., Václavík V., Řepka M., Bendová M. (2013). A proposal for simplifying the method of evaluation of uncertainties in measurement results. Measurement Science Review, 13 (1), pp. 1–6.
12. UNI EN 1925 (2000). Natural stone test methods - Determination of water absorption coefficient by capillarity. Rome: CNR-ICR.
13. UNI EN 13755 (2008). Natural stone test methods - Determination of water absorption at atmospheric pressure. Rome: CNR-ICR.